

Porosity and volume assessments of large wood (LW) accumulations

Gabriel Spreitzer^{a,*}, Jon Tunnicliffe^b, Heide Friedrich^a

^a Department of Civil & Environmental Engineering, University of Auckland, Auckland, New Zealand

^b School of Environment, University of Auckland, Auckland, New Zealand

ARTICLE INFO

Article history:

Received 20 September 2019

Received in revised form 24 January 2020

Accepted 25 February 2020

Available online 26 February 2020

Keywords:

Large wood (LW) accumulations

LW mapping in rivers

Structure from Motion (SfM) photogrammetry

Poisson mesh reconstruction

LW volume

LW porosity

ABSTRACT

The formation of large wood (LW) accumulations during floods represents a major hazard for constricted river cross-sections, e.g. bridges and weirs, as it affects flow hydraulics and sediment transport. To better assess LW accumulations, reliable strategies and techniques are required. There are currently practical limits on monitoring accumulation configurations. Both laser scans and photogrammetric techniques can be used to scan the outer contours of LW accumulations, but cannot practically assess the wood content and porosity. Details of the outer deposit are captured in high resolution, but the core of the deposit remains occluded, and estimation is necessary. This becomes more challenging for deposits of increasing size (relative to wood elements). To develop a more efficient workflow for LW accumulation assessment in the field, we performed a laboratory study to develop a relationship between the envelope volume of water-worked LW jams during a single flood hydrograph and the volume of woody elements within (explicitly accounting for porosity). We used photogrammetric techniques, now in common use for reconnaissance surveys of debris accumulations, on wood accumulations scaled for the laboratory. The study's aim is to develop a semi-automated assessment method, enabling efficient image acquisition, processing and computation of LW accumulation volume. Using a multi-camera array above the laboratory channel, and applying Structure from Motion photogrammetry, we developed 3D models for 16 experimental flow-formed wood accumulations, each with >50 individual wooden dowels. No correlations were found between porosity and flow magnitude; porosity was found to be similar for most deposits (~66%). As a result of this accumulation structure, the envelope volume used in 3D and 2.5D photogrammetric methods tended to overestimate wood content by 3× and 2.6×, respectively. The results obtained here will contribute to a more reliable volumetric assessment for inventories of wood mass in river systems.

© 2020 Elsevier B.V. All rights reserved.

1. Introduction

1.1. Large wood (LW) accumulations in rivers

Management concerns regarding large wood (LW) in rivers are raised more frequently in New Zealand (Cave et al., 2017; Phillips et al., 2018) and other parts in the world (Ruiz-Villanueva et al., 2019), especially in steep forested catchments, where in-stream wood may exhibit dynamic transport and accumulation processes during floods (Naiman et al., 2002; Comiti et al., 2016; Spreitzer et al., 2019a). While abundance of LW in stream systems is a natural component of fluvial habitats and ecosystems (Wohl et al., 2016), exceptionally high rates of in-stream wood, which is often produced by natural disasters (e.g. wind through, fires, snow avalanches, landslides) or forestry activities, poses a hazard for river crossing infrastructure (Piegay et al., 1999; Lassette and Kondolf, 2012; Schmocker and Weitbrecht, 2013), and

human populations as a consequence of obstructed infrastructure (Mazzorana et al., 2011; Comiti et al., 2016; Gschnitzer et al., 2017). Once LW enters the channel, it may be mobilised and transported downstream, strongly depending on log geometries in relation to flow depth (Bilby and Ward, 1989; Abbe et al., 1993). Often the transported LW ends up in an accumulation together with smaller organic fine material (OFM) and sediments, showing a broad range of packing ratios inside the accumulation matrix (porosity). Previous research has shown that LW accumulation formation and frequency is strongly influenced by channel width, log diameter, log length, forest type and age (Likens and Bilby, 1982; Gregory et al., 1993; Gurnell et al., 2002; Abbe and Montgomery, 2003; Warren et al., 2009).

Flow magnitude (Ruiz-Villanueva et al., 2016c) and channel obstructions at constricted cross-sections, such as at bridge piers (Rusyda, 2015; Panici and de Almeida, 2018), standing vegetation (Gurnell et al., 2002; Bertoldi et al., 2013; Bertoldi et al., 2015), and already existing LW formations in the channel (Abbe and Montgomery, 1996; Welber et al., 2013; Bertoldi et al., 2014), are assumed to be dominant factors for the formation of LW jams, besides the available quantity of LW (Keller and Swanson, 1979) and its transport regime (e.g.

* Corresponding author.

E-mail addresses: gspr390@aucklanduni.ac.nz (G. Spreitzer), j.tunnicliffe@auckland.ac.nz (J. Tunnicliffe), h.friedrich@auckland.ac.nz (H. Friedrich).

uncongested, congested and hypercongested (Braudrick et al., 1997; Ruiz-Villanueva et al., 2019)). Depending on the packing matrix, LW accumulations are posing high risk to redirect flow as 'deflector jams' (Abbe and Montgomery, 2003; Lassetre and Kondolf, 2012), reshaping of channel-bed topography, including scouring processes beneath an accumulation (Melville and Dongol, 1992; Schalko et al., 2019b) and sedimentation in the upstream reach of the obstruction (Marston, 1982; Mao et al., 2008; Spreitzer et al., 2018; Spreitzer et al., 2020b in Review). Beyond a certain threshold of channel obstruction and interweaving of woody elements, detectable backwater effects begin to occur. The effects of LW accumulations on backwater buildup have been studied (Hartlieb, 2017; Schalko et al., 2019a), yet variations in composition and proportion of retained materials, as well as accumulation porosity, are difficult to quantify for existing LW obstructions. Previous studies found that backwater effects develop as a consequence of stream power reduction (Knauss, 1995; Ruiz-Villanueva et al., 2016b), conveyance loss (Gippel et al., 1996; Gschnitzer et al., 2017) and roughness of LW (Maser et al., 1988; Buffington and Montgomery, 1999). However, interstitial space inside an accumulation body has to be accounted for, as well, and this can change due to dynamic forces (e.g. compression and relaxation) and clogging processes with additional retained materials (Livers et al., 2015). In general, four types of LW accumulations have been identified (Wallerstein et al., 1997), each showing variation in composition and packing matrix that affect flow hydraulics and channel morphology. Accumulation porosity is an important parameter for the assessment of jam formations, from monitoring to modelling (Manners et al., 2007; Boivin and Buffin-Bélanger, 2010), and varies significantly across studies. While a few studies have estimated log jam porosity to be in a range of 13 to 90% (Thevenet et al., 1998; Sanhueza et al., 2019), most studies revealed porosity parameters between 25 and 70% (Livers et al., 2015; Dixon, 2016). Log geometry governs porosity of accumulation skeletons, while the packing matrix varies with the aspect ratio (e.g. diameter/length) of the structural members (Zhang et al., 2006; Li et al., 2010).

Depending on moisture content density, and age of wooden pieces (Ruiz-Villanueva et al., 2016a), an entire LW accumulation can float during flood events, while settling and changing its structure with decreasing water level. Both scenarios, floating as well as settled LW accumulations, may affect flow and channel morphology for each of the flow regimes, as LW accumulation porosity changes. Investigations into log retention and jam formation at bridge piers and decks have revealed important insights into accumulation processes (Diehl, 1997; Gschnitzer et al., 2017; De Cicco et al., 2018; Panici and de Almeida, 2018). A laboratory study conducted by Schalko et al. (2019b) in particular demonstrates the effects of a floating dowel accumulation on scour development at a LW retention rack. However, there is still limited understanding of the characteristic packing arrangements for a given LW structure (e.g. compactness (ratio of solid matter to the bulk volume), porosity (ratio of void volume to the bulk volume)), especially in the presence of high drag resistance (peak discharge) and during the relaxation phase at the recession limb of a hydrograph. Estimating LW accumulation porosity is challenging, as precise information about accumulation volumes is required.

1.2. Mapping of LW accumulations

Although the importance and need for volumetric measures of LW accumulations have been frequently addressed in literature (Harmon et al., 1986; Lienkaemper and Swanson, 1987; Gurnell et al., 2002; Webb and Erskine, 2003; Manners and Doyle, 2008; Dixon and Sear, 2014; Wohl and Scott, 2017; Martin et al., 2018), accurate assessment methods available for the estimation of LW volume and accumulation porosity, are limited to date (Spreitzer et al., 2019b). Conventional volumetric methods often consider manually obtained measurements of individual logs (Cordova et al., 2006; Andreoli et al., 2007; Manners et al., 2007; Brown et al., 2014; Dixon and Sear, 2014; Tonon et al.,

2018), or entire accumulations by means of a 'rectangular' approach, measuring the bounding-box of the accumulation body in form of a parallelepiped (Thevenet et al., 1998; Andreoli et al., 2007; Boivin et al., 2015). These methods provide an initial, rough estimation of bulk volume, yet they are not effective for complex log formations, nor applicable and safe for accumulations in rugged environments or non-wadable streams. Airborne surveys, via light aircraft or unmanned aerial vehicle (UAV) (Casado et al., 2015; Rusnák et al., 2018), present a highly advantageous platform for surveying with high resolution image sensors or LiDAR systems (Rusnák et al., 2018; Sanhueza et al., 2019); this approach has become more popular and affordable in recent years.

UAV-based photogrammetry provides great potential for mapping of LW accumulations, yet the resolution has to be sufficiently detailed to resolve individual LW pieces in the point cloud model (Spreitzer et al., 2019b), and distinguish between gravel and wood particles of similar optical characteristics (Colvard, 1998; Wright et al., 2000). A variety of volumetric techniques are available to progress from a high-density point cloud to a volumetric mesh model. By generating the convex hull of the points, it is possible to estimate the volume by voxel techniques (Moskal and Zheng, 2011; Hosoi et al., 2013) or other geometric estimation methods, such as cutting the object into thin slices along the z-axis (Chang et al., 2017), and '2.5D' volumetric techniques, which are based on the vertical projection of the convex hull of the point clouds onto a 2D raster grid (Remondino, 2003; Sanhueza et al., 2019). The relationship between 2.5D models, 3D meshes, and the true geometric volume of the wood deposit is difficult to assess, particularly for over-arching geometries and complex 3D forms. As the size of the accumulation grows, relative to stem diameter and length, there is a proportional increase in the volume of 'occluded' material that cannot be determined from topographic surveys.

Mapping of LW accumulations, including volumetric assessment and porosity estimates, is challenging due to the complex nature of jam formations, typically comprising a LW skeleton (Manners and Doyle, 2008), and void spaces which can be empty or filled with OFM and sediments (Thevenet et al., 1998; Linstead, 2001). Therefore a robust image-based methodology, leading to a high quality point cloud model, will provide a high level of detail in surface texture and geometries (Westoby et al., 2012; Dikovski et al., 2014; Micheletti et al., 2015), and can significantly increase the success rate of Structure from Motion (SfM) photogrammetry for LW applications. A high-quality model will provide accurate accumulation volume and porosity estimates.

High variability in surface texture and geometry is beneficial for SfM photogrammetry point-matching algorithms (Maiti and Chakravarty, 2016). However, complex geometries (e.g. multiple intersections of individual elements, or protruding logs and branches) can also cause the reconstruction algorithm to fail (Spreitzer et al., 2019b). A rich variety of surface textures (e.g. grass, sediment, wood) is advantageous for LW accumulation mapping, as colour filtering can be used to classify components of the accumulation. Orru et al. (2016) used colour segmentation from surface texture to gain information about spatial and temporal changes in relative proportions of sand and gravel particles in a flume study. Furthermore, contrasting surface textures can help to reveal void volume within the accumulation, where observable from the surface (Glasbey et al., 1991; Anovitz and Cole, 2015). Methods to determine area and volume of voids have previously been established in the field of crystalline materials (Turner et al., 2011). Attempts to estimate porosity of soil samples have employed SfM photogrammetry, geometrical models, and water displacement methods, however, further innovations are required to achieve a more reliable outcome (Seitz et al., 2018).

Recent advances in survey technologies have allowed researchers to capture topographic details quickly, safely and with remarkable accuracy and resolution. New survey techniques, such as LiDAR and SfM, make it possible to resolve LW accumulations with spatial resolutions in the range of 150 points/m² to 1 point/mm² (Boivin and Buffin-Bélanger, 2010; Tonon et al., 2014; Grigillo et al., 2015). SfM has been

demonstrated to deliver point-cloud accuracy that is roughly similar to that of LiDAR (Mancini et al., 2013; Kaiser et al., 2014; Ružić et al., 2014), at a much lower cost, although it is not able to penetrate leafy vegetation and tree canopy in the way that LiDAR does.

1.3. Objectives

Our aim is to assess the volumetric characteristics of relatively coarse LW accumulations that consist mainly of large structural members. By forming woody deposits in a flume environment, we can reproduce the packing arrangement of natural, water-worked structures, albeit with only the major 'skeletal' elements and none of the finer organic detritus. By comparing three volume estimation approaches, we can assess the magnitude of 'occluded geometry' within the core of complex accumulation models, which is beyond the reach of lasers and optical sensors. Assessing the porosity of LW accumulations is important for in-stream wood inventories, as well as assessing the hydraulic characteristics of channel-spanning structures. Less porous structures reduce river flow capacity, leading to backwater effects (overbank flooding) and flow diversion towards banks.

We present a solid SfM photogrammetry workflow, such as recently introduced in the course of a laboratory study, using manually assembled miniature log piles for volume and porosity estimates (Spreitzer et al., 2020a), that can significantly contribute to an improved assessment strategy of LW accumulation volume, porosity as well as wood characteristics, which have been identified as important research goals for future LW projects by Pagliara and Carnacina (2010) and Gschnitzer et al. (2017). In the present study, we increased model complexity by using water worked LW accumulations in a flume setup and assessed log jam volume and porosity from aerial-like imagery exclusively. Furthermore, we identify and reconstruct arrangement and packing structures of major structural elements, which differs from the matrix of slash, willows and finer material that eventually fill in interstitial space in the log-formation. Finding the characteristic porosity of the structural members presents a challenging problem, given the dynamic nature of river stage: volume estimates taken during low stage may be different from conditions at high flow. The deposit may become more tightly enmeshed when material is floating and/or compressed by river flows, while porosity may increase with the relaxation processes during falling water levels. This study provides an essential contribution to the data acquisition and processing stage of a systematic assessment framework, which is urgently needed by river managers, engineers and researchers (Wohl et al., 2016), to better understand and manage LW accumulations in rivers.

2. Experimental setup

2.1. Hydraulic flume

In the Water Engineering Laboratory at the University of Auckland, a 6 m long and 1.5 m wide hydraulic flume with conveyor-belt feeder, live-bed conditions, floating material screen and sediment trap was used to perform LW accumulation experiments (Fig. 1a and b). The flume is fully integrated into an automated pump system, with a pressure head of 10 m and electro-magnetic flow meters, allowing for graded flow conditions without intermission. The experimental setup is fully geometrically scaled at a ratio of 1:15 for in-stream elements (4–63 mm gravel), as well as simulated LW (wooden dowels), and inclined to a slope of 0.02, typical of an upland gravel-bed river reach. The 75 mm thick active layer of the channel ranges between 0.8 and 1.0 m in width over a slightly meandering course, and is limited by fixed embankments (8–16 mm gravel-cement-mixture). Channel banks show an average height of 200 mm. The flume is equipped with floats, which function as point gauges to measure water levels (sheltered from floating wood) at multiple cross-sections along the channel.

Situated 4 m downstream from the inlet, a bridge (1.5 m long, 240 mm wide) crosses the channel; this represents a constricted cross-section in our laboratory environment, and its central row of piers is prone to the formation of LW accumulations. The constricted cross-section was set up with a free board of 240 mm between bridge deck and channel bed. The row of piers consists of three cylindrical piles, each 20 mm in diameter.

A 0.55 m wide and 3 m long conveyor-belt was used for feeding sediment and LW into the channel at the inlet section of the flume. The feeding system is operated via 12 V DC motor and an intermediate gear box, reducing conveyor-belt speed while increasing torque and input accuracy. A control panel with potentiometer allows for speed control. The discharging speed varies between 3 and 17 mm s⁻¹. Transported bedload along the flume channel is collected at a downstream screen (25 mm grid raster for filtering floating materials e.g. wooden dowels) and a bedload trap; both are situated at the flume outlet.

2.2. Wooden dowels

In the course of our LW accumulation experiments, we used wooden dowels made from *Pinus radiata* (Monterey pine). The dowels have a mean density of 0.5 g cm⁻³, similar to wood densities for LW in full-scale river systems (Ruiz-Villanueva et al., 2016a), and are commonly used for experiments in a flume environment (Braudrick and Grant, 2000). The cylindrical dowels represent wood logs in their simplest form (e.g. no rootwad, branches), comparable to de-limbed and topped tree stems that are introduced as a result of forestry operations. The dowels were categorized into three size classes and spray-painted according to length and diameter (see Table 1). The dowels had diameters ranging from 6 to 28 mm, and lengths that ranged between 67 and 533 mm (Fig. 1d). The smallest class is considered as 'fine LW', representing woody pieces with a prototype length between 1.0 and 1.5 m and a diameter ranging from 0.09 to 0.15 m. Very large woody pieces are considered as 'coarse LW', representing prototype tree boles 6.0 and 8.0 m in length and 0.18 to 0.42 m in diameter. All organic material in-between fine and coarse LW is considered as 'standard LW'. Five 'design' dowels, with individual colour code (green, yellow, blue, purple and red), were mixed into the sample for additional analysis and verification purposes of the applied methodology. The five design dowels represent a prototype wood log with a length of 4 m and diameter of 0.33 m.

2.3. Imaging and recording equipment

For LW accumulation mapping in the flume, a multi-camera array, consisting of five high-resolution cameras, was installed on a mobile platform above the channel (Fig. 1b and c). The platform runs on rails along the longitudinal axis of the flume. Four cameras were aligned in square-formation, each edge length being 125 mm, inclined by 15° from the vertical and focusing towards the channel centreline, with a fifth camera positioned centrally above the channel. The camera array covers the entire flume width, oriented such that there is no <84% image overlap. All cameras are linked to a computer via USB and controlled by a software algorithm in Visual Studio Code, which allows for adjustment of camera parameters and time-controlled image capture. The cameras were developed by e-con Systems (Model: See3Cam CU130) and are equipped with a 13 MP image sensor and a 5.5 mm lens, allowing for Ultra HD (4 K) resolution at a maximal horizontal field of view of 58°. The CMOS electronic rolling shutter image sensor, lens and high-performance image signal processor chip are mounted on a compact (30 × 30 mm) module board. All the cameras maintain a fixed focus, which was set manually for each camera to achieve the best alignment with the flume environment. To allow for optimal light conditions in the flume, and for elimination of shade from any external

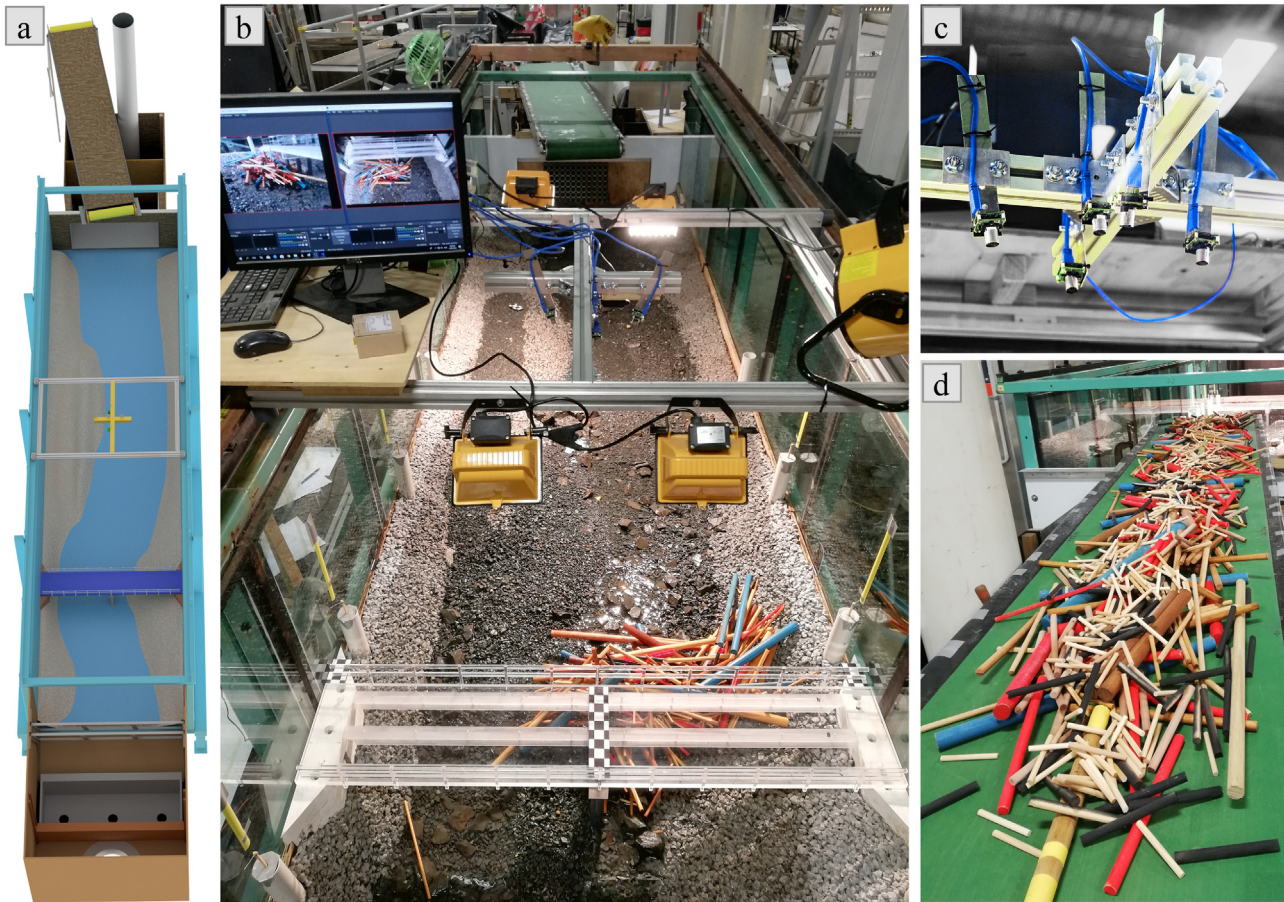


Fig. 1. Experimental setup in the Water Engineering Laboratory at the University of Auckland.

light sources, four 500 W halogen lights were installed on the mobile platform facing the flume centre.

In addition to the multi-camera array, two Microsoft Logitech webcams were installed to record all experiments. One webcam is positioned at the inlet, facing downstream, whereas the other webcam captures the bridge section from top.

Table 1
Overview of dimension and quantity of the wooden dowels used in the experimental setup.

Classification	Dowel dimension		Number of dowels		Colour code
	Length (mm)	Diameter (mm)	521Pcs.	1769 Pcs.	
Fine	67	6	210	1050	Natural
	100	10	–	310	Black
Standard	133	10	90	90	Natural
	200	8	39	39	Red
		12	39	39	Red
	267	22	6	6	Red
		28	3	3	Red
		8	51	69	Natural
12		51	108	Natural	
Coarse	400	22	15	18	Natural
		22 Design Dowel	5	5	Green, Yellow, Blue, Purple, Red
	533	28	3	7	Natural
		12	–	8	Natural
		18	–	3	Blue
		22	6	7	Natural
28		3	3	Blue	
26	18	–	2	Natural	
	26	–	2	Blue	

3. Methodology

3.1. Experimental procedure

At the outset of the flume experimentation, two calibration runs were carried out. Three of the five design dowels, which were manually placed in the channel, were used to assess the performance of the photogrammetry method for individual and paired wooden dowels. Mapping of individual dowels reduces the effects of void spaces and enables net volume computation of the dowel. For the paired dowel formation, one dowel was placed with perpendicular orientation on top of the other one. These two initial calibration experiments were performed in order to capture volumetric properties, which are fundamental for the assessment of accumulation porosity (Fig. 2a-e).

The experimental series consisted of 23 flume runs, with either 521 or 1769 wooden dowels. The dowels were divided into three equally-sized lots (one per meter conveyor-belt-length, see Fig. 1d), and fed via conveyor-belt system at a constant speed of 17 mm s^{-1} . The experimental hydrograph consisted of a base discharge of 4 L s^{-1} , gradually ramping up to a peak discharge of either 20 , 50 or 75 L s^{-1} and then back to base discharge again, over a period of seven minutes for each experimental run. The first ten runs, each releasing 521 dowels into the channel flow, had a peak discharge of 20 L s^{-1} . Ten further runs (again with 521 dowels) were then conducted with a magnitude of 50 L s^{-1} . Next, another three runs, each involving 1769 dowels, were tested with a peak discharge of 75 L s^{-1} .

Experiments were declared successful if a minimum number of 50 wooden dowels became lodged in an accumulation at the bridge pier. Successful flume runs were designated as

LW Accumulations - Composition and Proportion Retained

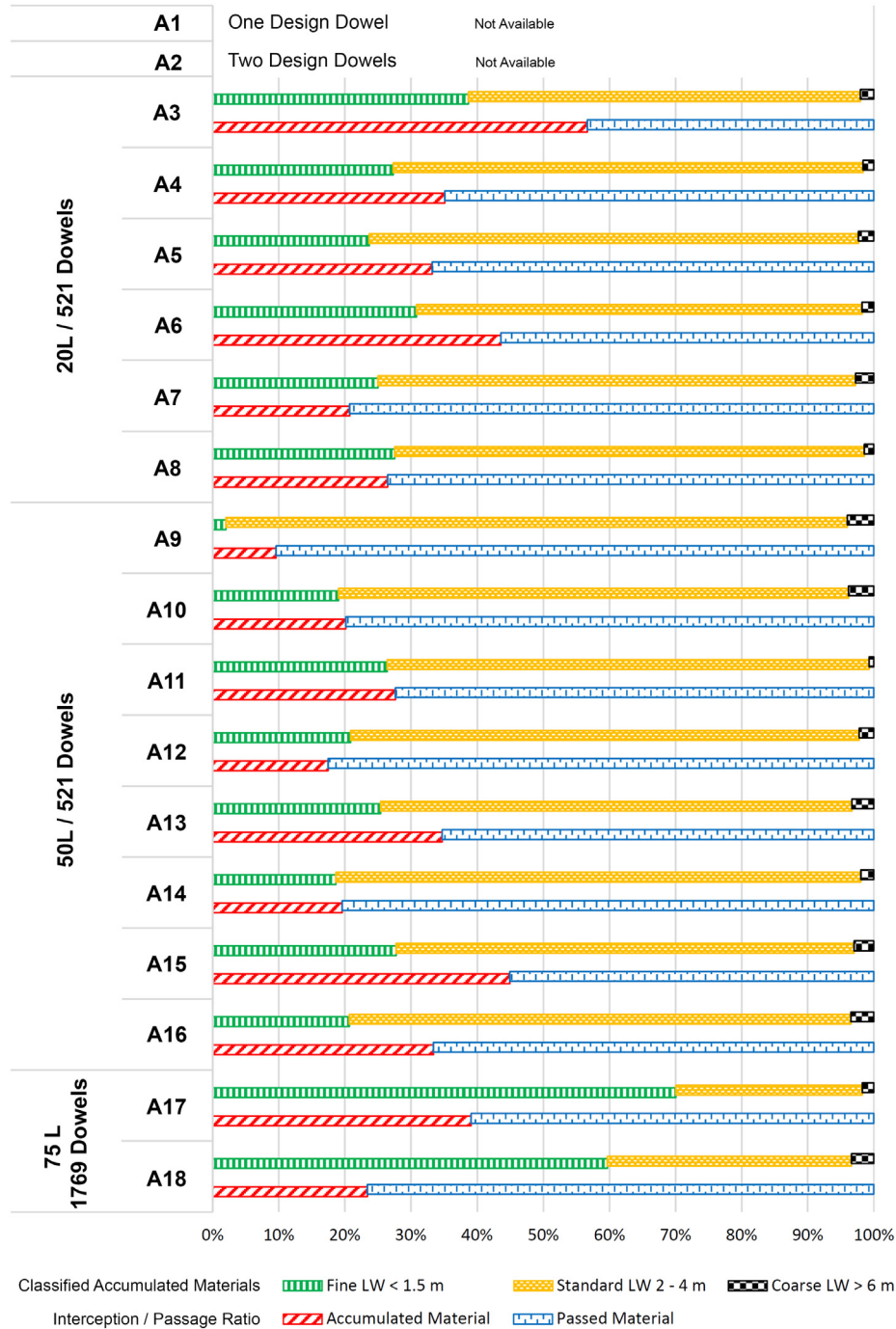


Fig. 2. Analysis of intercepted materials at the critical cross-section (bridge pier), with passing ratio set relative to the total introduced wood (number of wood dowels). LW material was classified into three groups: fine LW (smaller than 1.5 m), standard LW (2 to 4 m in length), and coarse LW (with a length of 6 m and longer).

accumulations (A) with sequential numbering. After each experimental run, the dowel accumulation was scanned via multi-camera array and then manually disassembled for documentation of the class and number of dowels. All the dowels by-passing the bridge section during the experimental runs were collected at the outlet screen.

3.2. Image acquisition

After each experimental run, the flume was drained and five checker boards, with a grid raster of 25 mm, were placed in the

area of interest. The flow-formed dowel accumulation was then scanned via multi-camera array. The platform was moved along the longitudinal axis of the flume, stopping at intervals of 50 mm to capture the 1.5 m long section. Each photographic dataset comprised a total of 150 images, which were obtained from 30 stations, covering the study reach with the bridge and LW accumulation. The time for each image collection and platform relocation interval was set to five seconds, allowing enough time to move the platform and save images to the computer. The survey method proved to be very efficient, requiring approximately five minutes per experiment.

3.3. Point cloud and mesh generation

Pix4Dmapper (Pix4D Switzerland, 2018), version 4.1.25, a commercially available SfM photogrammetry software package, was used for point cloud generation. The datasets, each comprising 150 heavily overlapping images of the dowel accumulation and bridge section in the flume, were added to a Pix4D project, in order to reconstruct the 3D scene. A camera-rig model was created for the five See3Cams of the multi-camera array, which was saved to the Pix4D database to guarantee the same initial camera parameters for all subsequent point cloud model generation.

Point cloud processing was achieved in three main steps: (i) initial tie point generation, (ii) point cloud densification and (iii) orthoimage and digital surface model (DSM) generation. Our image acquisition method used the processing template '3D Maps' for model generation, since four of the cameras were inclined by 15° from the vertical. The first processing step produced results in an arbitrary coordinate system, aligned with the flume (longitudinal axis of the flume (x), lateral axis (y) and vertical axis (z)), since no geodetic data are available in the laboratory. Before point cloud densification, the initial tie point cloud is scaled, using the checker boards placed in the reach. For the best scaling outcome, we ensured multiple scaling constraints for each camera model per checker board. Other point cloud processing settings were kept as default, allowing for optimal point density and good surface detail, which are important for subsequent surface reconstruction (meshing). Processing times varied between 2 and 4 h for initial point cloud generation, 1 to 2 h for point cloud densification and a few minutes for DSM and Orthoimage generation.

The densified point cloud model was then imported into CloudCompareV2 (2016) version 2.6.3, to isolate the points comprising the LW accumulation from background features using the 'Segmentation' tool. It has been shown that this tool works particularly well for LW photogrammetry and point cloud processing applications (Spreitzer et al., 2019b), as segmentation is easily possible with the polygonal lasso tool. In order to pre-clean the point cloud selection, we applied statistical outlier removal (SOR) employing six immediate neighbour points for mean distance estimation.

After segmentation, the LW accumulation point cloud model was imported into MeshLab (Cignoni et al., 2008) version 2016.12, for point normal computation and screened Poisson surface reconstruction (PSR). Point normals were estimated with respect to their surface position, taking consideration of the closest 60 points for each point in the 3D point cloud, which provided the best performance for the randomly arranged cylindrical dowels. The initial surface meshing was then conducted using PSR, with a reconstruction depth of 12. PSR (Kazhdan et al., 2006; Kazhdan and Hoppe, 2013) has proven to be very robust to noise, and a reliable surface reconstruction algorithm (Wolff et al., 2016). We used a scale factor of 1.0, and kept all further parameters as default, showing an adaptive octree depth of five, conjugate gradient depth of zero, minimum number of samples of 1.5, and an interpolation weight of four for the screened Poisson equation.

Faces were filtered according an optimum threshold of edge length; values ranged between 5 and 10 mm, depending on model complexity. This criteria for face selection was used to avoid creating holes in the accumulation surface, whilst removing large faces that were generated at the edges of the accumulation during the PSR meshing procedure. All non-manifold faces, and isolated pieces smaller than 10% of the largest of the mesh pieces, were filtered out of the mesh model. Any holes in the model surface were then closed. The final mesh models showed a large number ($\sim 10^6$) of faces. To achieve a more efficient workflow, the relatively big mesh models were simplified to a maximum number of 10^5 faces. This was achieved via a re-meshing process: Quadric Edge Collapse Decimation in MeshLab, using a target number of 100,000 faces. Our simplification procedure further considered the optimal position of vertices and post-simplification cleaning at a quality threshold of

0.3. The resulting accumulation models maintained rich surface features at a reasonable face count.

Because neither PSR, nor the 'Close Hole' algorithm in MeshLab, are able to close the bottom of the accumulation models, the simplified mesh models were imported into Meshmixer (2018) version 3.5.474. Meshmixer is a freely available mesh editing software from Autodesk, especially designed for triangle meshes. The 'Erase and Fill' tool allows for the selection of the mesh edge and closing of the mesh bottom. Our workflow used the smooth MVC (mean value coordinates) setting, without refining or smoothing the model. This procedure in Meshmixer enabled the creation of entirely closed 'watertight' accumulation mesh models, which are essential for determining 3D volume of the accumulation model (Wang et al., 2018).

3.4. Accumulation assessment

Three approaches for volume estimation of LW accumulations were employed. First, a 3D geometric volume of each accumulation was assessed based on the quantity of dowels in each size class, and their respective lengths and diameters. Next, SfM photogrammetry was used to assess 2.5D and 3D model volume. 2.5D volume estimates are a well-established technique for volumetric estimates in industry and geosciences based on digital elevation models (DEMs) (Milan et al., 2007; Lague et al., 2013; Steeb et al., 2017; Nourbakhshbeidokhti et al., 2019). Pix4Dmapper offers a 2.5D approach for volume estimates (Pix4Dmapper, 2018). The accuracy depends on the model resolution, which is interpreted as ground sampling distance (GSD). The 2.5D volume (henceforth referred to as referred to as '2.5D Pix4D Volume') is computed by integrating the product of GSD and vertical distances from individual basal grid elements to the top of the mesh model surface. The generation of a basal grid involves interpolating the most likely ground topography beneath the accumulation; this is straightforward in the laboratory, but would be more complex in the field.

We have previously shown that 2.5D volume does not consider void space inside of LW accumulations and only accounts for a very limited amount of void space accessible from the surface (Spreitzer et al., 2020a). For this reason, elaboration of 3D models could be more beneficial and may present a means to increase accuracy of volumetric assessment in LW research. Our procedure for the generation of mesh models for LW accumulations has been outlined above, and considers the entire mesh editing and processing pipeline by means of freely-available meshing software packages (e.g. CloudCompare, MeshLab, Meshmixer). To compute geometric measures for 3D volume estimation, the watertight accumulation models were imported into MeshLab. Here, the volumetric result, based on PSR meshing, is designated as the '3D PSR Volume'.

Subtracting the 3D geometric volume (3D, geo) from the computed bulk volumes (2.5D or 3D, PSR), provides an assessment of accumulation porosity. Porosity was estimated for both the 2.5D model (Eq. (1)) and the 3D model (Eq. (2)), as a ratio of void volume (V_v) over total volume (bulk volume, V_{tot}). LW accumulations are complex and a certain level of randomness applies to the depositional behaviour. Based on the uniform cylindrical shape of our applied dowels, with aspect ratios (L/D ; dowel length L , and diameter D) varying from 7 to 33, the expected porosity of disordered (random) packing arrangements (showing 50 and more dowels), is lower than 85% and higher than 35%, according to mathematical models (Zou and Yu, 1996; Rahli et al., 1999; Zhang et al., 2006; Liu et al., 2018), with a typical porosity of $60 \pm 10\%$. To date, the lowest achievable porosity of cylinder accumulations is 9.31% (does not consider entrapped OFM, sediments, etc.), with regards to the densest packing arrangement of circles in a 2D plane (Trovato et al., 2007).

$$n_{2.5D} = \frac{V_v}{V_{tot}} = 100 \frac{V_{2.5D, Pix4D} - V_{3D, geo}}{V_{2.5D, Pix4D}} (\%) \quad (1)$$

$$n_{3D} = 100 \frac{V_{3D,PSR} - V_{3D,geo}}{V_{3D,PSR}} (\%) \quad (2)$$

4. Results

Two initial tests (A1 and A2), for verification of the SfM photogrammetry methodology, were conducted with dry conditions in the flume. The first 10 flume runs introduced 521 dowels at a peak discharge of 20 L s^{-1} ; 60% of these resulted in sizeable LW accumulations (>50 dowels) and were declared successful (A3 to A8). In the next 10 runs (50 L s^{-1}), 80% of the experiments were considered to be successful (A9 to A16). The final set of experiments introduced 1769 dowels at a peak discharge rate of 75 L s^{-1} . Two out of the three experiments (A17 and A18) were considered to be successful. In the course of our experiment, we observed changes in packing arrangements of the water-worked LW accumulations at different stages along the simulated flood hydrograph.

4.1. LW interception and passing rate

Run A7 resulted in the smallest accumulation (108 dowels; 21% of the feed) of the first experimental runs (521 dowels at 20 L s^{-1}). Run A3 retained the most wooden dowels, showing an interception ratio of 57% (295 dowels). The distribution of fine LW in the accumulations varied between a quarter and a third of the supplied wood, while standard sized dowels made up the rest, for this series of experimental runs (Fig. 2).

Accumulations A9 to A16, with a peak discharge of 50 L s^{-1} , intercepted a minimum of 50 (A9) up to a maximum of 234 dowels (A15). This experimental series showed similar accumulation ratios to the experiments using 20 L s^{-1} , with only one exception, accumulation A9, which retained 94% of standard LW in the accumulation. The smallest accumulation also contained the smallest number of fine LW pieces (2%), and resulted in the lowest interception ratio of 10%. Of interest is the relatively high interception ratio (4%) of coarse LW for the smallest dowel formation, amongst all the others.

The number of dowels for the accumulations A17 and A18 ranged from 414 up to 691 dowels. Results further revealed high amounts of fine LW, in both dowel accumulations (60 and 70%), at a ratio of 2 to 3% for coarse LW.

4.2. LW accumulation volume and porosity

We computed 2.5D and 3D volumes of dowel accumulation structures, which had been formed by a range of flow magnitudes. The first two calibration tests were performed with individual (A1; Fig. 3a, c and i) and paired design dowels (A2; Fig. 3e, g and i), which were manually placed in the channel and scanned via multi-camera array. The test using one design dowel revealed a 2.5D Pix4D volume of $0.115 \cdot 10^{-3} \text{ m}^3$, and 3D PSR volume computation resulted in $0.104 \cdot 10^{-3} \text{ m}^3$. The 3D geometric volume of one design dowel was calculated to $0.102 \cdot 10^{-3} \text{ m}^3$. 2.5D volume for the paired design dowels resulted in $0.313 \cdot 10^{-3} \text{ m}^3$, while the 3D PSR volume showed $0.241 \cdot 10^{-3} \text{ m}^3$. Volumetric results allow for estimation of accumulation porosity using Eqs. (1) and (2). Porosity estimates based on the 2.5D approach, Eq. (1), revealed 11% for a single dowel (A1) and 35% for the paired dowels (A2), as shown in Fig. 4. In contrast, the 3D PSR volumes resulted in porosity parameters of 2% for accumulation A1 (Fig. 3d) and 16% for A2 (Fig. 3h).

Throughout the course of the experiments, 16 water-worked dowel accumulations were formed, strongly varying in volume, across all flow magnitudes. Accumulations formed by the lowest flow magnitude had 3D geometric volumes ranging from 2.92 (A8) to $5.54 \cdot 10^{-3} \text{ m}^3$ (A3), see Table A.1. For accumulations formed at a discharge of 20 L s^{-1} , the computed 3D PSR volume varied from 6.56 to $14.74 \cdot 10^{-3} \text{ m}^3$. The 2.5D Pix4D approach resulted in volumes ranging from 7.00 to $16.50 \cdot 10^{-3} \text{ m}^3$. At a discharge of 50 L s^{-1} , 3D geometric volume varied from 1.90 (A9) to $5.72 \cdot 10^{-3} \text{ m}^3$ (A15) with a computed 3D PSR volume ranging from 3.89 to $15.58 \cdot 10^{-3} \text{ m}^3$, and 2.5D Pix4D volume 4.75 to $16.26 \cdot 10^{-3} \text{ m}^3$. Accumulation volumes from both experimental series of runs, using 20 and 50 L s^{-1} , showed large variations in size, offering no clear correlation between flow magnitudes and accumulation volume. Accumulations A17 and A18 were formed at a flow magnitude of 75 L s^{-1} showing a reference volume of 8.78 and $7.18 \cdot 10^{-3} \text{ m}^3$. 3D PSR volume for the largest of our water worked accumulations resulted in 22.84 and $22.01 \cdot 10^{-3} \text{ m}^3$, which was again slightly overestimated from the 2.5D Pix4D approach (28.24 and $24.51 \cdot 10^{-3} \text{ m}^3$). Detailed volumes are presented in Table A.1.

With increasing 3D geometric volume, volumetric deviations increase for both the 2.5D Pix4D and 3D PSR method. Deviations related to the 3D PSR approach range from 2 (A1) up to 67% (A18), while the 2.5D Pix4D method shows larger deviations for every accumulation. These deviations are a measure of accumulation porosity, according to Eqs. (1) and (2). Differences between the 2.5D and 3D PSR approaches were significant for elementary and smaller accumulation structures

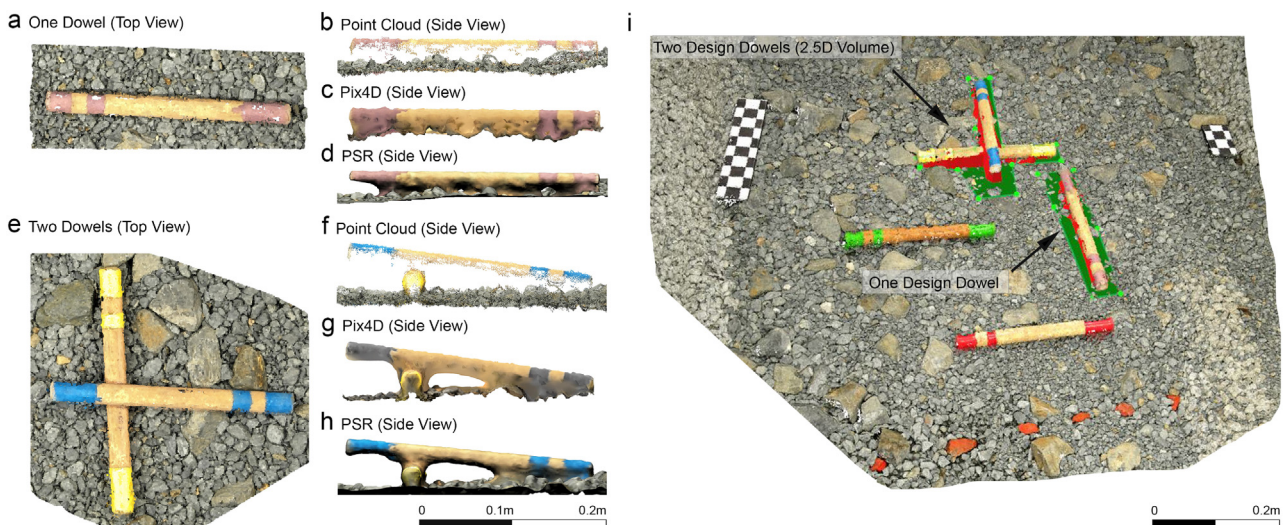


Fig. 3. Point cloud models of a single design dowel (a), from a side perspective (b) and for Pix4D mesh (c) and PSR model (d). A top view of paired design dowels from top view (e), point cloud with from side view (f) and the mesh model in Pix4D (g) as well as PSR (h). Volume estimates in Pix4D for individual and paired dowels are displayed on the right (i).

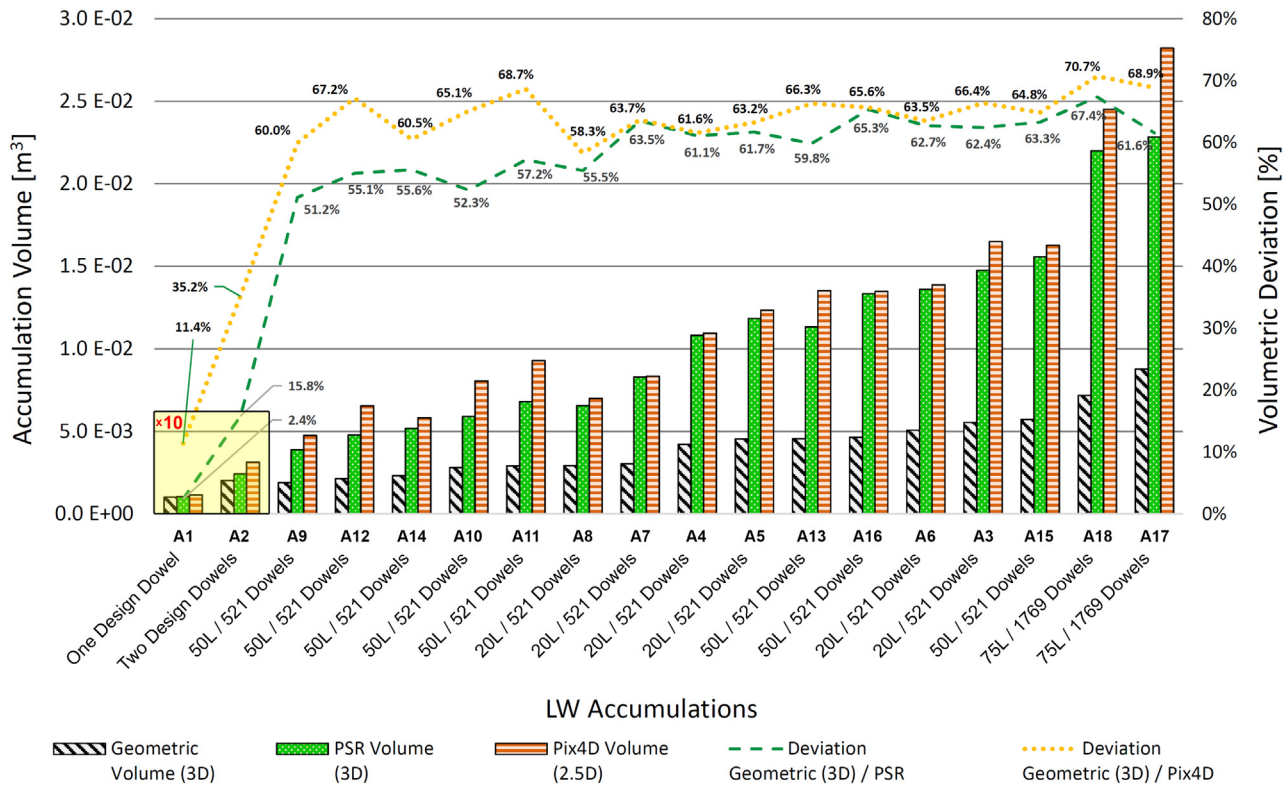


Fig. 4. Volumetric results of the experimental LW accumulations are ranked in order of increasing geometric volume (3D). Accumulation volumes A1 and A2 are magnified by a factor of 10. Other LW accumulations were generated by a 20, 50 or 75 L s⁻¹ (L) discharge and had a feed of either 521 or 1769 dowels (A3 to A18).

(10 to 20%), with a decreasing trend as 3D geometric volumes increase. In the course of our experiments, deviations settled between the 60 and 70% range (Fig. 4).

5. Discussion

5.1. Assessment of water-worked LW accumulations

5.1.1. Depositional rates of scaled wooden dowels

The difference in LW dowel count, between smallest and largest dowel accumulation, was 187 dowels for experiments with a peak discharge of 20 L s⁻¹, and 184 dowels for 50 L s⁻¹. The dowel accumulations that formed at 20 and 50 L s⁻¹ in the flume environment showed log counts that were consistent with field studies in the north-eastern United States: 20 LW accumulations were studied, which comprised 20 to 305 individual LW pieces (Thompson, 2012). Experiments A17 and A18 were run with a maximum magnitude of 75 L s⁻¹ and a total wood load of 1769 dowels, according to Table 1. The overall interception ratios align with our previous experiments, using a flow magnitude of 20 and 50 L s⁻¹: see Fig. 2 (60–70% fine LW, 2–3% coarse LW).

Each of the dowel accumulations (A3 to A18) comprised coarse LW pieces, ranging from 1 to 4% (by count) with regards to the entire dowel accumulation. Coarse LW, in particular very long wood pieces in relation to channel width, have been shown to significantly influence accumulation behaviour (Keller and Swanson, 1979; Lienkaemper and Swanson, 1987). In total, between 10 and 57% (Fig. 2) of the entire dowel feed accumulated immediately upstream of the bridge; all formations were initiated by the bridge pier. These relatively large interception ratios align with observations in the field, where massive LW jams developed in the course of a single flood event (Lucía et al., 2015; Cave et al., 2017; Phillips et al., 2018). The largest number of dowels were intercepted during experiments that applied a peak discharge of 20 L s⁻¹, whereas the lowest number of dowels resulted from a discharge of 50 L s⁻¹.

The two experiments that led to the development of a dowel accumulation at 75 L s⁻¹ (A17 and A18), revealed interception rates of approximately one third of the entire available wood load.

There was a difference of only one dowel between accumulation A5 (20 L s⁻¹), and A16 (50 L s⁻¹), compare Table A.1. Similar dowel count at different discharges were also found for accumulations A4 and A13 (two dowels), as well as A7 and A10 (three dowels). Marked variations in accumulation complexity across the full range of experimental discharges were observed, offering no clear correlation between flow magnitude and interception rate. None of our experiments resulted in a channel-spanning blockage, which was not unexpected, as all of the dowels were shorter than the channel width, and accumulated at a restricted cross-section in the channel (Diehl, 1997; Mazzorana et al., 2011; Panici and de Almeida, 2018). Furthermore, literature reveals that accumulation behaviour depends on existing obstructions in the channel and wood characteristics (e.g. rootwads, branches) (Abbe and Montgomery, 1996; Braudrick and Grant, 2001), whereas the wooden dowels in this study had the simplest possible geometry; no rootwads or branches, and clean cuts, such as often found in New Zealand stream systems. LW accumulation processes are strongly driven by complex flow regimes and wood geometries (Manners et al., 2007; Gschnitzer et al., 2017; Schalko et al., 2019b), which still require extensive research to better predict log deposition and accumulation formation processes.

5.1.2. Accumulation volume vs dowel count

Previous studies have revealed that high flow events may redistribute LW in channels, while removing old wood and depositing new material in existing LW accumulations (Lienkaemper and Swanson, 1987). Although redistribution occurs in our experiments, similar structures are formed in the course of each flood event (Evans et al., 1993). Despite the similar mode of formation, there was no clear correlation between flow magnitude and the size of dowel accumulation. Accumulations A17 and A18 retained up to almost three times the number of dowels as previous experiments, and the 3D geometric volumes (7.18 to 8.78

10^{-3} m^3), as well as the 2.5D and 3D PSR volumes, were consistent with the trend of previous experiments.

Because of the different size classes of dowels used, the 3D geometric volume does not exactly coincide with the number of dowels that make up the accumulations. A7 shows a larger volume than A8, despite being comprised of fewer dowels, at a flow magnitude of 20 l s^{-1} . The same applies to accumulations A4 and A5. Due to log orientation and geometric alignment complexities 'packing matrix' during the accumulation processes (Braudrick and Grant, 2001; Abbe and Montgomery, 2003), differences in 3D geometric volume may be relatively small ($< 4\%$ or $0.1 \cdot 10^{-3} \text{ m}^3$), while the computed volumes can show variations of 16 to 20% ($\sim 1.5 \cdot 10^{-3} \text{ m}^3$) (compare A7 and A8 (20 L s^{-1}) in Table A.1). This effect was also observed for accumulations formed at higher discharge rates of 50 L s^{-1} : compare accumulation A13 and A16, as well as across the flow magnitudes. Accumulation A11 (50 L s^{-1}) retained 144 dowels, which is 36 more than A7 (20 L s^{-1}), and yet A7 shows a larger 3D geometric volume. The opposite is observed for accumulations A3 ($5.54 \cdot 10^{-3} \text{ m}^3$) and A15 ($5.72 \cdot 10^{-3} \text{ m}^3$) at flow magnitudes of 20 and 50 L s^{-1} , (Table A.1). A3 shows the smallest volume of the two, whilst having 61 dowels less than A15. However, we found individual cases that show similar 3D geometric, as well as 3D PSR volumes (A8 and A11) and 2.5D Pix4D volumes (A7 and A10; A13 and A16; see Table A.1).

Results revealed that the computed 3D PSR volume correlates very well to the number of accumulated dowels, with only one major exception, accumulation A17. The number of elements comprising a LW accumulation can significantly contribute to the complexity of the accumulation skeleton (Shields, 2001; Pagliara and Carnacina, 2010; Thompson, 2012), containing more void spaces at the inside of the jam formation, which are difficult to capture. Our experiments, ranging from 20 to 75 l s^{-1} , revealed an evenly related proportional deviation scale with the size of the accumulation, for both the 2.5D and 3D assessment techniques (Fig. 4 and Fig. 5).

5.1.3. 2.5D vs 3D assessment

In each of our experiments, the 3D geometric volume was overestimated by the 3D PSR method, and even further overestimated by the 2.5D Pix4D method, which was expected (Spreitzer et al., 2020a). This is also consistent with the assumptions inherent in the 2.5D approach (Verbree and Van Oosterom, 2003; Pix4DMapper, 2018). Absolute differentials between 3D PSR and 2.5D Pix4D volumes generally reached values of up to $2.5 \cdot 10^{-3} \text{ m}^3$ (A11 and A18), with a maximum of $5.4 \cdot 10^{-3} \text{ m}^3$ (A17), indicating clearly that in all of our experiments the 3D PSR approach performed better in capturing volumes. The reason for the improved performance of the 3D method is, again, related to the higher fidelity capture of void spaces from all angles of the accumulation surface (Glasbey et al., 1991; Lian et al., 2012). Overhanging features and void spaces at the periphery of the deposit are not resolved when applying the 2.5D approach (Jones et al., 2008; Spreitzer et al., 2020a).

The 3D PSR approach performed reasonably accurately for a single dowel A1 (102% of 3D geometric volume), however, the 2.5D Pix4D approach more severely overestimated the reference 3D geometric volume (113%; compare A1 and A2 in Table A.1). For the paired wooden dowels (A2), deviations from the reference arose for both methods, although the deviations in the case of the 3D PSR approach were less (119%) than those from the 2.5D Pix4D approach (154%). Porosity for these elementary structures are slightly larger than observed in previous laboratory studies on LW accumulation volumes (Spreitzer et al., 2020a). More complex LW accumulations revealed higher deviation (detailed parameters on the overestimation are presented in Table A.1), while accumulation A18 showed a maximum for the 3D PSR (306%) as well as 2.5D Pix4D approach (341%). This overestimation is most likely related to nadir image acquisition - as obtained in aerial surveys, such as taken from drones (Rusnák et al., 2018), helicopters (Dietrich, 2016) and planes (Smikrud and Prakash, 2006) - compared

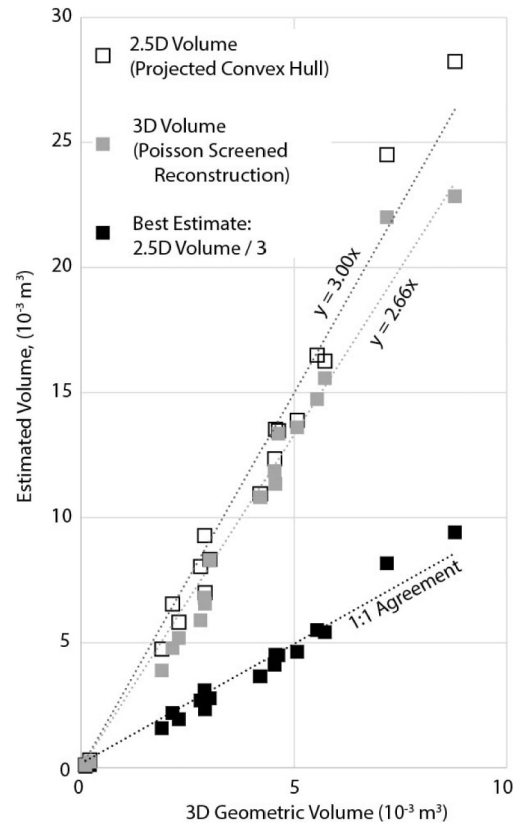


Fig. 5. The relationship between 3D Geometric Volume (volume of individual dowels) versus two techniques for estimating the envelope volume of the deposit. The 2.5D technique consistently provides about three times the geometric volume, whereas the 3D PSR technique conforms more closely to the deposit and has a lower volume. This relationship provides a means of determining the porosity of the deposit: about 66% void space, according to the 2.5D technique.

to 'oblique' images captured from various sub-vertical angles, as used in previous studies (Rossi et al., 2017; Spreitzer et al., 2019b; Spreitzer et al., 2020a).

In the present study we found that the 2.5D technique consistently provides about three times '3x' the 3D Geometric Volume (a regression yields $R^2 = 0.98$; see Fig. 5), providing a practical guideline for photogrammetric work on water-worked accumulations that consist mainly of larger, structural members. A porosity of $\sim 66\%$, represents a fairly typical value for such deposits in LW literature (Livers et al., 2015; Dixon, 2016), though it is likely an upper boundary for porosity in coherent LW accumulations. Our porosity estimates for the accumulation skeletons, using a SfM photogrammetry approach, are consistent with porosity approximations in mathematical models of cylindrical rods with similar aspect ratios (Liu et al., 2018; Freeman et al., 2019). As interstitial material accumulates within the deposit, void space will tend to decrease; see Sanhueza et al. (2019). A power relationship can be considered (most upper estimates sit above the trend line; an exponent of ~ 1.22 provides a better fit), but we used a linear trend here for the limited range of accumulation volumes we tested.

5.1.4. LW accumulation compression and relaxation

In assessing the formation of the dowel accumulations, it was observed that the packing structure changed, during the waning stage of each run. In the present work we defined the 'relaxation' process as the settling of recently jammed wooden elements (the LW accumulation) with dropping water levels. The opposite effect was called 'compression'. During peak discharge, dynamic forces acting on LW elements (Manners et al., 2007; Shields and Alonso, 2012) may transform the nature of the structure. Medium density and wood moisture

content (often related to wood age) affect the buoyancy of the wooden material (Ruiz-Villanueva et al., 2016a), resulting in floating LW accumulations, similar to the experimental setup of a recent study on LW retention structures (Schalko et al., 2019b).

In our study, compression and relaxation effects correspond with flood magnitude (Fig. 6). Individual dowels (marked-up ellipses), which are embedded into the accumulation, were identified and tracked to reveal compression and relaxation processes at varying discharge rates. Compression and alignment processes were observed with increasing flow magnitude (compare Fig. 6a to c). At peak discharge, the accumulation reached a stagnation point, resulting in a stable dowel accumulation. With decreasing water level, the LW accumulation experienced a longitudinal expansion in the upstream direction, reaching a relaxation point at base discharge (4 L s^{-1}). The relaxation point at the rising limb was reached at 50 L s^{-1} , see stagnation and relaxation line in Fig. 6b, c and f.

Identifying compression and relaxation processes of LW accumulations at varying flow magnitudes is important to better understand and assess log formations, as the structure of the accumulation body may change in terms of porosity that could affect discharge behavior at the restricted cross-section (Heede et al., 1972; Gregory et al., 1985; Pagliara and Carnacina, 2010; Gschnitzer et al., 2017; Schalko et al., 2018) and channel morphology (Keller and Swanson, 1979; Gippel et al., 1996). Accordingly, at high flow conditions, LW accumulations

may show a higher compactness than at a stage of low discharge (Manners et al., 2007), and at a time when LW accumulations are usually assessed.

5.2. Practical outcomes

Porosity estimates can be effectively obtained for elementary accumulation structures using SfM photogrammetry (Spreitzer et al., 2020a), however, currently available surface reconstruction algorithms are limited in providing deeper insight into complex LW accumulations. Our experiments have shown that the number of dowels incorporated into an accumulation linearly align with accumulation porosity for both the 3D PSR and the 2.5D Pix4D approach. With increasing accumulation size and dowel count, however, porosity estimates become more difficult and vague using solely SfM photogrammetry. This is a similar observation to the 'rectangular approach', which considers the air-wood volume.

The 2.5D model approach was shown to provide a reliable and efficient tool for bulk volume estimation (Pix4Dmapper, 2018), and outperforms conventional approaches of rough volumetric estimates based on log count and measurements (Cordova et al., 2006; Tonon et al., 2018), as well as the air-wood rectangular approach introduced and used by Piegay (1993), Boivin et al. (2015) and Lucía et al. (2015). The 3D PSR model approach considered some of the accessible

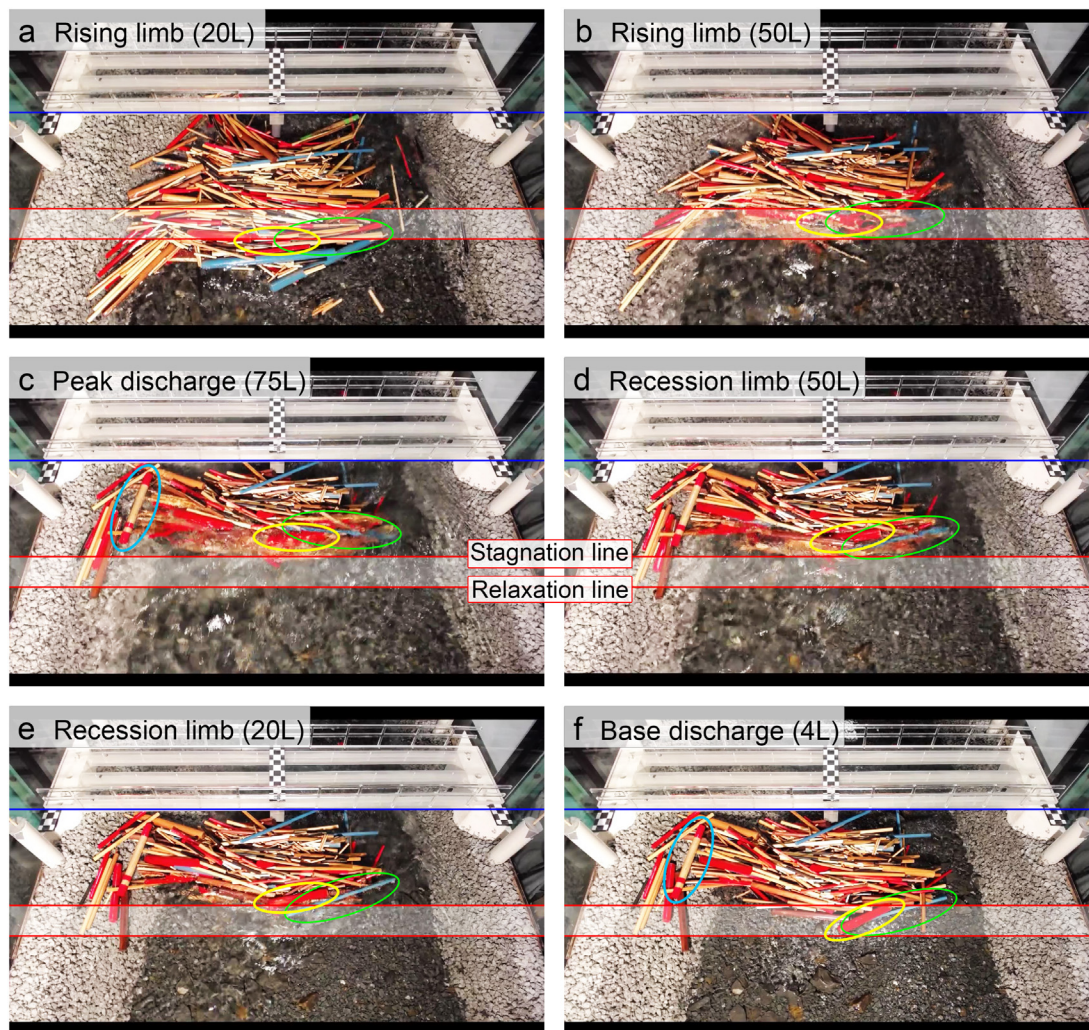


Fig. 6. Development of a LW accumulation (A17) consisting of individual dowels starting from the rising limb at 20 L s^{-1} (20L) in (a), reaching peak discharge 75 L s^{-1} (75L) in (c), and the falling limb back to base discharge 4 L s^{-1} (4L) in (f), at the critical cross section (bridge with central pier) from top view perspective. The blue line indicates a reference line at the bridge, whereas the two red lines indicate the relaxation area of the LW accumulation during recession from peak discharge (c) to base discharge 4 L s^{-1} (f).

overhanging void spaces (Carrea et al., 2015), resulting in somewhat more accurate volume computation than 2.5D Pix4D.

As our laboratory studies have revealed, currently available techniques enable accurate surface reconstruction, yet the SfM photogrammetry workflow could not effectively capture the porosity from 3D models due to a lack of more deeply oblique and sub-vertical images of the accumulation (Rossi et al., 2017; Vacca et al., 2017). With the application of more advanced meshing algorithms, such as have been applied in the reconstruction of vegetation (Hosoi et al., 2013; Raunonen et al., 2013; Hackenberg et al., 2015; Hétroy-Wheeler et al., 2016), the workflow presented here could be significantly improved. These meshing algorithms may enable more complete detection of LW elements in an accumulation, enabling a fuller reconstruction of the log skeleton, similar to the mesh model of A17, displayed in Fig. 7. Porous space inside the bounded region may then be determined on the basis of geometric relations and properties from two and three dimensional surfaces, revealing accessible void spaces (Virgin et al., 1996; Thovert et al., 2001; Sumanasooriya et al., 2010). These algorithms could furthermore help to reconstruct irregular porous structures (Naderi et al., 2019), providing more precise porosity estimates, as well as quantifying OFM. Such advances are helpful for tasks such as in-stream wood inventories, or setting boundary conditions for hydraulic modelling (Manners et al., 2007; Pagliara and Carnacina, 2010; Lai, 2016).

Our initial calibration test, using two design dowels for calibration, clearly revealed the effects of a lack of oblique and lateral images, showing an overestimation in volume by 15.8% (Fig. 4), whereas almost identical volumes were achieved for a similar setup with sufficiently high photo count of aerial 'nadir' and oblique images (Spreitzer et al.,

2020a), also see Fig. 8. As our image datasets in this manuscript exclusively considered aerial images, which resulted in considerable volume deviations, we recommend the use of a mixture of aerial and side-looking images to better resolve LW accumulations (Rossi et al., 2017; Vacca et al., 2017). This may be of particular importance for large log formations in the channel, which have been registered during aerial flights, yet require a larger image count in order to increase model accuracy for LW accumulation assessment (Steeb et al., 2017).

Experimental results show that even for these elementary LW accumulations, the applied PSR method cannot fully resolve the occluded geometry from aerial photogrammetry models. With this experimental study we show that the 3D approach performs slightly better than the 2.5D approach, yet the achieved outcome, considering exclusively aerial image datasets, is not sufficiently accurate for reliable volumetric assessment. However, based on the 3D geometric volume and the computed volumes, estimates of LW accumulation porosity can be made (Fig. 5). Given the accessibility of aerial/UAV photogrammetric techniques, we anticipate that further improving the relationship between envelope volume and the porosity of water-worked LW accumulation structures will be an important frontier in further LW inventory work.

In providing more information about void spaces inside of LW accumulations, which represent a substantial part of the deposit that potentially affects flow hydraulics (Manners et al., 2007; Pagliara and Carnacina, 2010), LW-related challenges such as backwater effects and flow diversion can be better tackled. The consistency in porosity of LW accumulation skeletons, such as revealed in this study with roughly 66%, may be used as a correction factor for pore space and finer debris for reconnaissance-scale work on LW inventories. Previous studies

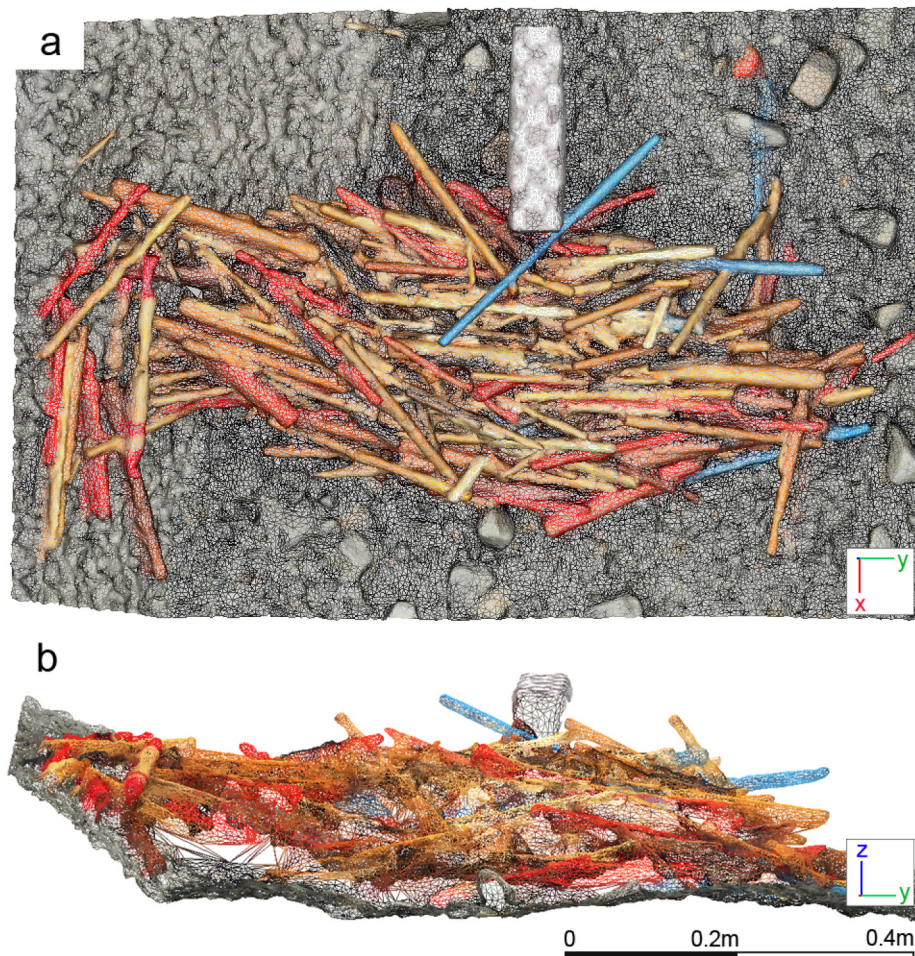


Fig. 7. Accumulation A17, displayed as mesh model in top (a) and front view (b).

but not the volume of constituent elements. LW accumulation porosity is likely to be underestimated when mapped during low flow magnitudes, due to observed compression (rising limb of the hydrograph + LW supply) and relaxation processes of the accumulation matrix at the recession limb of the hydrograph.

Our experimental findings provide evidence that both 2.5D and 3D photogrammetric techniques are beneficial for estimating LW accumulation volume, and we provided a first correlation between 3D geometric volume, computed volumes (2.5D, 3D) and jam porosity for complex log skeletons. Both tested techniques represent efficient tools that allow for surface mapping and the generation of LW accumulation models, which are of importance for future approximations of the hidden mass under the surface of LW accumulations. We found that the 3D PSR approach performed better in capturing volumetric information than the 2.5D Pix4D method; in particular for elementary accumulation structures, as void spaces, which are accessible from the surface, are not considered by the 2.5D approach. However, perhaps of greater importance is developing a robust relationship between envelope volume (however determined) and the volume of woody elements (compactness) or void spaces (porosity). This will vary with the composition of the deposit, and thus a range of compositional types should be explored, in a range of river environments.

Appendix A. Appendix

Table A.1

Results of the volumetric estimates for the formed dowel accumulations in the laboratory. Deviations for 3D PSR and 2.5D Pix4D volumes are computed with respect to the 3D Geometric volume.

Accumulation	Flow magnitude ($L s^{-1}$)	3D geometric volume (10^{-3})	3D PSR volume (10^{-3})	2.5D Pix4D volume (10^{-3})	Over-estimation 3D PSR (%)	Over-estimation 2.5D Pix4D (%)	Number of dowels (pcs.)
A1	–	0.102	0.104	0.115	102	113	1
A2	–	0.203	0.241	0.313	119	154	2
A3	20	5.54	14.74	16.50	266	298	295
A4	20	4.21	10.82	10.96	257	260	183
A5	20	4.54	11.85	12.35	261	272	173
A6	20	5.07	13.60	13.89	268	274	227
A7	20	3.03	8.30	8.34	274	275	108
A8	20	2.92	6.56	7.00	225	240	138
A9	50	1.90	3.89	4.75	205	250	50
A10	50	2.81	5.89	8.05	210	287	105
A11	50	2.91	6.80	9.29	234	319	144
A12	50	2.15	4.78	6.55	223	305	91
A13	50	4.56	11.35	13.53	249	297	181
A14	50	2.30	5.18	5.82	225	253	102
A15	50	5.72	15.58	16.26	272	284	234
A16	50	4.63	13.35	13.48	288	291	174
A17	75	8.78	22.84	28.24	260	322	691
A18	75	7.18	22.01	24.51	306	341	414

References

- Abbe, T.B., Montgomery, D.R., 1996. Large woody debris jams, channel hydraulics and habitat formation in large rivers. *Regulated Rivers: Research & Management* 12, 201–221.
- Abbe, T.B., Montgomery, D.R., 2003. Patterns and processes of wood debris accumulation in the Queets river basin, Washington. *Geomorphology* 51, 81–107.
- Abbe, T.B., Montgomery, D.R., Fetherston, K.L., McClure, E., 1993. A process-based classification of woody debris in a fluvial network: preliminary analysis of the Queets River, Washington. *EOS Transactions AGU* 74, 296.
- Andreoli, A., Comiti, F., Lenzi, M.A., 2007. Characteristics, distribution and geomorphic role of large woody debris in a mountain stream of the Chilean Andes. *Earth Surf. Process. Landf.* 32, 1675–1692.
- Anovitz, L.M., Cole, D.R., 2015. Characterization and Analysis of Porosity and Pore Structures. *Rev. Mineral. Geochem.* 80, 61–164.
- Bertoldi, W., Gurnell, A.M., Welber, M., 2013. Wood recruitment and retention: the fate of eroded trees on a braided river explored using a combination of field and remotely-sensed data sources. *Geomorphology* 180–181, 146–155.
- Bertoldi, W., Welber, M., Mao, L., Zanella, S., Comiti, F., 2014. A flume experiment on wood storage and remobilization in braided river systems. *Earth Surf. Process. Landf.* 39, 804–813.
- Bertoldi, W., Welber, M., Gurnell, A.M., Mao, L., Comiti, F., Tal, M., 2015. Physical modelling of the combined effect of vegetation and wood on river morphology. *Geomorphology* 246, 178–187.
- Bilby, R.E., Ward, J.W., 1989. Changes in characteristics and function of woody debris with increasing size of streams in Western Washington. *Trans. Am. Fish. Soc.* 118, 368–378.
- Boivin, M. & Buffin-Bélanger, T. 2010. Using a terrestrial lidar for monitoring of large woody debris jams in gravel-bed rivers. *7th Gravelbed Rivers Conference, 5–10 September 2010, Tadoussac, Quebec, Canada* (poster).
- Boivin, M., Buffin-Bélanger, T., Piégay, H., 2015. The raft of the Saint-Jean River, Gaspé (Québec, Canada): a dynamic feature trapping most of the wood transported from the catchment. *Geomorphology* 231, 270–280.
- Braudrick, C.A., Grant, G.E., 2000. When do logs move in rivers? *Water Resour. Res.* 36, 571–583.
- Braudrick, C.A., Grant, G.E., 2001. Transport and deposition of large woody debris in streams: a flume experiment. *Geomorphology* 41, 263–283.
- Braudrick, C.A., Grant, G.E., Ishikawa, Y., Ikeda, H., 1997. Dynamics of wood transport in streams — a flume experiment. *Earth Surf. Process. Landf.* 22, 669–683.
- Brown, A., McBroom, M., Zhang, Y., 2014. Developing a large woody debris budget for the lower San Antonio River. *Texas Water Development Board* 258.
- Buffington, J.M., Montgomery, D.R., 1999. Effects of hydraulic roughness on surface textures of gravel-bed rivers. *Water Resour. Res.* 35, 3507–3521.

Our work contributes to a better understanding of LW accumulations in stream systems. The 2.5D assessment technique provides an efficient workflow for rapid LW accumulation assessment, while the 3D PSR technique is more labour intensive, but provides higher resolution and more accurate volume estimates. The work presented in this article further addresses the need for interdisciplinary approaches, such as advances in mesh computation algorithms, that allow for the generation of LW accumulation skeletons and a significant improvement of the proposed SfM photogrammetry assessment technique.

Acknowledgements

The authors acknowledge funding received from the George Mason Centre for the Natural Environment and the Engineering New Zealand Rivers Group. Furthermore, we want to thank Dr. Francesco Comiti and a second anonymous reviewer for the constructive feedback received, which helped us to improve the quality of this manuscript.

Declaration of competing interest

The authors declare that they have no known competing financial interests or personal relationships that could have appeared to influence the work reported in this paper.

- Carrea, D., Abellan, A., Derron, M.-H. & Jaboyedoff, M. 2015. Automatic rockfalls volume estimation based on terrestrial laser scanning data. 425–428.
- Casado, M.R., Gonzalez, R.B., Kriechbaumer, T., Veal, A., 2015. Automated identification of river hydromorphological features using UAV high resolution aerial imagery. *Sensors (Basel)* 15, 27969–27989.
- Cave, M., Davies, N., Langford, J., 2017. Cyclone cook slash investigation 2017 report. Gisborne District Council - Land and Soil Environmental Services and Protection 121.
- Chang, W. C., Wu, C. H., Tsai, Y. H. & Chiu, W. Y. 2017. Object volume estimation based on 3D point cloud. *2017 International Automatic Control Conference (Cacs)*, 5.
- Cignoni, P., Callieri, M., Corsini, M., Dellepiane, M., Ganovelli, F. & Ranzuglia, G. 2008. MeshLab: an open-source mesh processing tool. *Proceedings of the 2008 Eurographics Italian Chapter Conference*.
- CLOUDCOMPAREV2 2016 CloudCompare V2, Version 2.6.3, Windows 64-bits.
- Colvard, J. R. 1998. Jamming in Yellowstone: Mapping Lagre Woody Debris in America's first National Park. *Master's Thesis on the Graduate School-NEW Brunswick Rutgers, The State University of New Jersey*, 60.
- Comiti, F., Lucía, A., Rickenmann, D., 2016. Large wood recruitment and transport during large floods: A review. *Geomorphology* 269, 23–39.
- Cordova, J.M., Rosi-Marshall, E.J., Yamamoto, A.M., Lamberti, G.A., 2006. Quantity, controls and functions of large woody debris in Midwestern USA streams. *River Res. Appl.* 13.
- De Cicco, P.N., Paris, E., Ruiz-Villanueva, V., Solari, L., Stoffel, M., 2018. In-channel wood-related hazards at bridges: A review. *River Res. Appl.* 34, 617–628.
- Diehl, T. 1997. Potential Drift Accumulation at Bridges. *U.S. Department of Transportation - Federal Highway Administration, FHWA-RD-97-028*, 52.
- Dietrich, J.T., 2016. Riverscape mapping with helicopter-based Structure-from-Motion photogrammetry. *Geomorphology* 252, 144–157.
- Dikovski, B., Lameski, P., Zdraveski, E. & Kulakov, A. 2014. Structure from motion obtained from low quality images in indoor environment. *Conference Paper - Vitola, Macedonia*, 4.
- Dixon, S.J., 2016. A dimensionless statistical analysis of logjam form and process. *Ecohydrology* 9, 1117–1129.
- Dixon, S.J., Sear, D.A., 2014. The influence of geomorphology on large wood dynamics in a low gradient headwater stream. *Water Resour. Res.* 50, 9194–9210.
- Evans, B.F., Townsend, C.R., Crowl, T.A., 1993. The retention of woody debris structures in a small stream following a large flood. *New Zealand Natural Sciences* 20, 35–39.
- Freeman, J.O., Peterson, S., Cao, C., Wang, Y., Franklin, S.V., Weeks, E.R., 2019. Random packing of rods in small containers. *Granul. Matter* 21.
- Gippel, C., O'Neill, I., Finlayson, B., Schantz, I., 1996. Hydraulic guidelines for the re-introduction and management of large woody debris in lowland rivers. *Regulated Rivers: Research & Management* 12, 223–236.
- Glasbey, C.A., Horgan, G.W., Darbyshire, J.F., 1991. Image analysis and three-dimensional modelling of pores in soil aggregates. *J. Soil Sci.* 42, 479–486.
- Gregory, K.J., Gurnell, A.M., Hill, C.T., 1985. The permanence of debris dams related to river channel processes. *Hydrol. Sci. J.* 30, 371–381.
- Gregory, K.J., Davis, R.J., Tooth, S., 1993. Spatial distribution of coarse woody debris dams in the Lynton Basin, Hampshire, UK. *Geomorphology* 6, 207–224.
- Grigillo, D., Vrečko, A., Mikoš, M., Gvozdanović, T., Anžur, A., Vežočanik, R., Petrovič, D., 2015. Determination of large wood accumulator in steep forested torrent using laser scanning. *Engineering Geology for Society and Territory* 3, 127–130.
- Gschntzer, T., Gems, B., Mazzorana, B., Aufleger, M., 2017. Towards a robust assessment of bridge clogging processes in flood risk management. *Geomorphology* 279, 128–140.
- Gurnell, A.M., Piegay, H., Swanson, F.J., Gregory, S.V., 2002. Large wood and fluvial processes. *Freshw. Biol.* 47, 601–619.
- Hackenberg, J., Spiecker, H., Calders, K., Dusek, M., Raunonen, P., 2015. SimpleTree – an efficient open source tool to build tree models from TLS clouds. *Forests* 6, 4245–4294.
- Harmon, M.E., Franklin, J.F., Swanson, F.J., Sollins, P., Gregory, S.V., Lattin, J.D., Anderson, N. H., Cline, S.P., Aumen, N.G., Sedell, J.R., Lienkaemper, G.W., Cromack, K., Cummins, K. W., 1986. Ecology of coarse woody debris in temperate ecosystems. *Adv. Ecol. Res.* 15, 133–302.
- Hartlieb, A., 2017. Decisive parameters for backwater effects caused by floating debris jams. *Open Journal of Fluid Dynamics* 7, 475–484.
- Heede, B.H., Forest, R.M., Station, R.E., 1972. *Flow and channel characteristics of two high mountain streams*, Rocky Mountain Forest and Range Experiment Station, Forest Service (U.S. Dept. of Agriculture).
- Hétroy-Wheeler, F., Casella, E., Boltcheva, D., 2016. Segmentation of tree seedling point clouds into elementary units. *Int. J. Remote Sens.* 37, 2881–2907.
- Hosoi, F., Nakai, Y., Omasa, K., 2013. 3-D voxel-based solid modeling of a broad-leaved tree for accurate volume estimation using portable scanning lidar. *ISPRS J. Photogramm. Remote Sens.* 82, 41–48.
- Jones, R.R., Wawrzyniec, T.F., Holliman, N.S., McCaffrey, K.J.W., Imber, J., Holdsworth, R.E., 2008. Describing the dimensionality of geospatial data in the earth sciences—recommendations for nomenclature. *Geosphere* 4, 354.
- Kaiser, A., Neugirg, F., Rock, G., Müller, C., Haas, F., Ries, J., Schmidt, J., 2014. Small-scale surface reconstruction and volume calculation of soil erosion in complex Moroccan gully morphology using structure from motion. *Remote Sens.* 6, 7050–7080.
- Kazhdan, M., Hoppe, H., 2013. Screened poisson surface reconstruction. *ACM Trans. Graph.* 32, 1–13.
- Kazhdan, M., Bolitho, M. & Hoppe, H. 2006. Poisson Surface Reconstruction. *Eurographics Symposium on Geometry Processing*, 10.
- Keller, E., Swanson, F.J., 1979. Effects of large organic material on channel form and fluvial processes. *Earth Surf. Process. Landf.* 4, 361–380.
- Knauss, J. 1995. *Von der oberen zur unteren Isar*, Versuchsanst. für Wasserbau und Wasserwirtschaft, Oskar-v.-Miller-Inst.
- Lague, D., Brodu, N., Leroux, J., 2013. Accurate 3D comparison of complex topography with terrestrial laser scanner: application to the Rangitikei canyon (N-Z). *ISPRS - Journal of Photogrammetry and Remote Sensing* 82, 10–26.
- Lai, Y.G., 2016. Quantitative modeling tools for large woody debris and other in-stream structures. *Reclamation - Managing Water in the West* 159.
- Lassetre, N.S., Kondolf, G.M., 2012. Large woody debris in urban stream channels: redefining the problem. *River Res. Appl.* 28, 1477–1487.
- Li, S., Zhao, J., Lu, P., Xie, Y., 2010. Maximum packing densities of basic 3D objects. *Chin. Sci. Bull.* 55, 114–119.
- Lian, Z.H., Godil, A., Rosin, P.L., Sun, X.F., 2012. A new convexity measurement for 3D meshes. *Ieee Conference on Computer Vision and Pattern Recognition (Cvpr) 2012*, 119–126.
- Lienkaemper, G.W., Swanson, F.J., 1987. Dynamics of large woody debris in streams in old-growth Douglas-fir forests. *Can. J. For. Res.* 17, 150–156.
- Likens, G., Bilby, R., 1982. Development and maintenance of organic debris dams in New England streams. In: Swanson, F.J., Janda, R.J., Dunne, T., Swanson, D.N. (Eds.), *Sediment Budgets and Routing in Forested Drainage Basins*. Pacific Forest and Range Experimental Station, Portland, OR, pp. 122–128.
- Linstead, C., 2001. The effects of large woody debris accumulations on river hydraulics and implications for physical habitat. *Hydro-ecology: linking Hydrology and Aquatic Ecology* 266, 91–99.
- Liu, L., Yuan, Y., Deng, W., Li, S., 2018. Evolutions of packing properties of perfect cylinders under densification and crystallization. *J. Chem. Phys.* 149, 104503.
- Livers, A., Lininger, K., Kramer, N. & Wohl, E. 2015. Porosity Problems. *Proceedings of Wood in World Rivers Conference, Padova, Italy*, June 2015.
- Lucía, A., Comiti, F., Borga, M., Cavalli, M., Marchi, L., 2015. Dynamics of large wood during a flash flood in two mountain catchments. *Nat. Hazards Earth Syst. Sci.* 15, 1741–1755.
- Maiti, A., Chakravarty, D., 2016. Performance analysis of different surface reconstruction algorithms for 3D reconstruction of outdoor objects from their digital images. *Springerplus* 5, 932.
- Mancini, F., Dubbini, M., Gattelli, M., Stecchi, F., Fabbri, S., Gabbianelli, G., 2013. Using Unmanned Aerial Vehicles (UAV) for high-resolution reconstruction of topography: the structure from motion approach on coastal environments. *Remote Sens.* 5, 6880–6898.
- Manners, R.B., Doyle, M.W., 2008. A mechanistic model of woody debris jam evolution and its application to wood-based restoration and management. *River Res. Appl.* 24, 1104–1123.
- Manners, R.B., Doyle, M.W., Small, M.J., 2007. Structure and hydraulics of natural woody debris jams. *Water Resour. Res.* 43.
- Mao, L., Andreoli, A., Comiti, F., Lenzi, M.A., 2008. Geomorphic effects of large wood jams on a sub-antarctic mountain stream. *River Res. Appl.* 24, 249–266.
- Marston, R.A., 1982. The geomorphic significance of log steps in forest streams. *Ann. Assoc. Am. Geogr.* 72, 99–108.
- Martin, D.J., Harden, C.P., Tran, L., Opavilowsky, R.T., 2018. Investigating patterns of in-channel wood deposition locations in a low gradient, variably-confined alluvial river system. *Prog. Phys. Geogr.* 42 (2), 139–161.
- Maser, C., Tarrant, R.F., Trappe, J.M., Franlin, J.F., 1988. *From the Forest to the Sea – A Story of Fallen Trees*. p. 153.
- Mazzorana, B., Hübl, J., Zischg, A., Largiadier, A., 2011. Modelling woody material transport and deposition in alpine rivers. *Nat. Hazards* 56, 425–449.
- Melville, B.W., Dongol, M.S., 1992. Bridge Pier Scour with Debris Accumulation. *J. Hydraul. Eng.* 118 (9), 1306–1310.
- MESHMIXER 2018. Autodesk Meshmixer - State-of-the-art software for working with triangle meshes. <http://www.meshmixer.com/>, Version 3.5.474.
- Micheletti, N., Chandler, J.H., Lane, S.N., 2015. Investigating the geomorphological potential of freely available and accessible structure-from-motion photogrammetry using a smartphone. *Earth Surf. Process. Landf.* 40, 473–486.
- Milan, D.J., Heritage, G.L., Hetherington, D., 2007. Application of a 3D laser scanner in the assessment of erosion and deposition volumes and channel change in a proglacial river. *Earth Surf. Process. Landf.* 32, 1657–1674.
- Moskal, L.M., Zheng, G., 2011. Retrieving forest inventory variables with Terrestrial Laser Scanning (TLS) in urban heterogeneous forest. *Remote Sens.* 4, 1–20.
- Naderi, S., Dean, J.S., Zhang, M., 2019. Three-dimensional virtual microstructure generation of porous polycrystalline ceramics. *Ceram. Int.* 45 (17), 21647–21656.
- Naiman, R.J., Balian, E. V., Bratz, K. K., Bilby, R. E. & Latterell, J. J. 2002. Dead Wood Dynamics in Stream Ecosystems. *USDA Forest Service Gen. Tech. Rep PSW-GTR-181*, 23–48.
- Nourbakhshbeidokhti, S., Kinoshita, A., Chin, A., Florsheim, J., 2019. A workflow to estimate topographic and volumetric changes and errors in channel sedimentation after disturbance. *Remote Sens.* 11, 586.
- Orru, C., Blom, A., Chavarrias, V., Ferrara, V., Stecca, G., 2016. A new technique for measuring the bed surface texture during flow and application to a degradational sand-gravel laboratory experiment. *Water Resour. Res.* 52, 7005–7022.
- Pagliara, S., Carnacina, I., 2010. Temporal scour evolution at bridge piers: effect of wood debris roughness and porosity. *J. Hydraul. Res.* 48, 3–13.
- Panici, D., De Almeida, G.A.M., 2018. Formation, growth, and failure of debris jams at bridge piers. *Water Resour. Res.* 54, 6226–6241.
- Phillips, C., Marden, M., Basher, L.R., 2018. Geomorphology and forest management in New Zealand's erodible steepplands: an overview. *Geomorphology* 307, 107–121.
- Piegay, H., 1993. Nature mass and preferential sites of coarse woody debris deposition in the lower Ain valley (Mollon Reach), France. *Regul. Rivers Res. Manag.* 8, 359–372.
- Piegay, H., Thevenet, A., Citterio, A., 1999. Input storage and distribution of large woody debris along a mountain river continuum the Drome River, France. *Catena* 35, 19–39.
- PIX4D SWITZERLAND 2018. Pix4Dmapper Pro - Educational, Version 4.1.25.
- PIX4DMAPPER 2018. Pix4Dmapper 4.1 - User Manual. 305.

- Rahli, O., Tadril, L., Blanc, R., 1999. Experimental analysis of the porosity of randomly packed rigid fibers. *Comptes Rendus de l'Académie des Sciences - Series IIB - Mechanics-Physics-Astronomy* 327, 725–729.
- Raunonen, P., Kaasalainen, M., Åkerblom, M., Kaasalainen, S., Kaartinen, H., Vastaranta, M., Holopainen, M., Disney, M., Lewis, P., 2013. Fast automatic precision tree models from terrestrial laser scanner data. *Remote Sens.* 5, 491–520.
- Remondino, F., 2003. From point cloud to surface the modeling and visualization problem. *International Archives of the Photogrammetry, Remote Sensing and Spatial Information Sciences*, XXXIV-5/W10, 11.
- Rossi, P., Mancini, F., Dubbini, M., Mazzone, F., Capra, A., 2017. Combining nadir and oblique UAV imagery to reconstruct quarry topography: methodology and feasibility analysis. *European Journal of Remote Sensing* 50, 211–221.
- Ruiz-Villanueva, V., Piegay, H., Gaertner, V., Perret, F., Stoffel, M., 2016a. Wood density and moisture sorption and its influence on large wood mobility in rivers. *Catena* 140, 182–194.
- Ruiz-Villanueva, V., Piegay, H., Gurnell, A.A., Marston, R.A., Stoffel, M., 2016b. Recent advances quantifying the large wood dynamics in river basins: New methods and remaining challenges. *Rev. Geophys.* 54, 611–652.
- Ruiz-Villanueva, V., Wyżga, B., Zawiejska, J., Hajdukiewicz, M., Stoffel, M., 2016c. Factors controlling large-wood transport in a mountain river. *Geomorphology* 272, 21–31.
- Ruiz-Villanueva, V., Mazzorana, B., Bladé, E., Bürkli, L., Iribarren-Anacona, P., Mao, L., Nakamura, F., Ravazzolo, D., Rickenmann, D., Sanz-Ramos, M., Stoffel, M., Wohl, E., 2019. Characterization of wood-laden flows in rivers. *Earth Surf. Process. Landf.* 44, 1694–1709.
- Rusnák, M., Sládek, J., Kidová, A., Lehotský, M., 2018. Template for high-resolution river landscape mapping using UAV technology. *Measurement* 115, 139–151.
- Rusya, M.I., 2015. Log jams at a bridge with a pier and a bridge without pier. *Procedia Engineering* 125, 277–283.
- Ružič, I., Marović, I., Benac, Č., Ilić, S., 2014. Coastal cliff geometry derived from structure-from-motion photogrammetry at Stara Baška, Krk Island, Croatia. *Geo-Mar. Lett.* 34, 555–565.
- Sanhueza, D., Picco, L., Ruiz-Villanueva, V., Iroumé, A., Ulloa, H., Barrientos, G., 2019. Quantification of fluvial wood using UAVs and structure from motion. *Geomorphology* 345, 106837.
- Schalko, I., Lageder, C., Schmockler, L., Weitbrecht, V., Boes, R.M., 2019b. Laboratory flume experiments on the formation of spanwise large wood accumulations: Part II – Effect on local scour. *Water Resour. Res.* 55 (6), 4871–4885.
- Schalko, I., Lageder, C., Schmockler, L., Weitbrecht, V., Boes, R.M., 2019a. Laboratory flume experiments on the formation of spanwise large wood accumulations: Part I – Effect on backwater rise. *Water Resour. Res.* 55 (6), 4854–4870.
- Schalko, I., Schmockler, L., Weitbrecht, V., Boes, R.M., 2018. Backwater rise due to large wood accumulations. *J. Hydraul. Eng.* 144, 04018056.
- Schmockler, L., Weitbrecht, V., 2013. Driftwood: risk analysis and engineering measures. *J. Hydraul. Eng.* 139, 683–695.
- Seitz, L., Haas, C., Noack, M., Wieprecht, S., 2018. From picture to porosity of river bed material using structure-from-motion with multi-view-stereo. *Geomorphology* 306, 80–89.
- Shields, F.D., 2001. Effect of Large Woody Debris Structures on Stream Hydraulics. From Proceedings of the conference on Wetland Engineering and River Restoration, Reno, Nevada, pp. 27–31.
- Shields, F.D., Alonso, C.V., 2012. Assessment of flow forces on large wood in rivers. *Water Resour. Res.* 48.
- Smikrud, K.M., Prakash, A., 2006. Monitoring large Woody Debris Dynamics in the Unuk River, Alaska using Digital Aerial Photography. *GIScience & Remote Sensing* 43, 142–154.
- Spreitzer, G., Friedrich, H. & Tunncliffe, J., 2018. Effects of a large woody debris accumulation on channel-bed morphology during flood events. *E3S Web of Conferences*, 40, 02024.
- Spreitzer, G., Gibson, J., Tang, M., Tunncliffe, J., Friedrich, H., 2019a. SmartWood: Laboratory experiments for assessing the effectiveness of smart sensors for monitoring large wood movement behaviour. *Catena* 182.
- Spreitzer, G., Tunncliffe, J., Friedrich, H., 2019b. Using Structure from Motion photogrammetry to assess large wood (LW) accumulations in the field. *Geomorphology* 346, 20.
- Spreitzer, G., Tunncliffe, J., Friedrich, H., 2020a. Large wood (LW) 3D accumulation mapping and assessment using structure from Motion photogrammetry in the laboratory. *J. Hydrol.* 581, 124430.
- Spreitzer, G., Tunncliffe, J. & Friedrich, H., 2020b. In Review. Initiation of upstream sediment deposition in the presence of large wood (LW) blockage: laboratory experiments. *Earth Surface Processes and Landforms*.
- Steeb, N., Rickenmann, D., Badoux, A., Rickli, C., Waldner, P., 2017. Large wood recruitment processes and transported volumes in Swiss mountain streams during the extreme flood of August 2005. *Geomorphology* 279, 112–127.
- Sumanasooriya, M., Bentz, D. & Neithalath, N., 2010. Planar image-based reconstruction of pervious concrete pore structure and permeability prediction. *ACI Materials Journal* 107-M48, 413–421.
- Thevenet, A., Citterio, A., Piegay, H., 1998. A new methodology for the assessment of large woody debris accumulations on highly modified rivers. *Regulated Rivers: Research & Management* 14, 467–483.
- Thompson, D.M., 2012. The challenge of modeling pool-riffle morphologies in channels with different densities of large woody debris and boulders. *Earth Surf. Process. Landf.* 37, 223–239.
- Thovet, J.F., Yousefian, F., Spanne, P., Jacquin, C.G., Adler, P.M., 2001. Grain reconstruction of porous media: application to a low-porosity Fontainebleau sandstone. *Phys. Rev. E Stat. Nonlinear Soft Matter Phys.* 63, 061307.
- Tonon, A., Picco, L., Ravazzolo, D., Lenzi, M.A., 2014. Using a terrestrial laser scanner to detect wood characteristics in gravel-bed rivers. *Journal of Agricultural Engineering* 45, 161.
- Tonon, A., Picco, L., Rainato, R., 2018. Test of methodology for developing a large wood budget: A 1-year example from a regulated gravel bed river following ordinary floods. *Catena* 165, 115–124.
- Trovato, A., Hoang, T.X., Banavar, J.R., Maritan, A., 2007. Symmetry, shape, and order. *Proc. Natl. Acad. Sci. U. S. A.* 104, 19187–19192.
- Turner, M.J., McKinnon, J.J., Jayatilaka, D., Spackman, M.A., 2011. Visualisation and characterisation of voids in crystalline materials. *CrystEngComm* 13, 1804–1813.
- Vacca, G., Dessì, A., Sacco, A., 2017. The use of nadir and oblique UAV images for building knowledge. *ISPRS Int. J. Geo Inf.* 6, 393.
- Verbree, E., Van Oosterom, P., 2003. The STN method: 3d-surface reconstruction by observation lines and Delaunay tets. *Commission III. WG 3*, 6.
- Virgin, B., Haslund, E., Hilfer, R., 1996. Rescaling Relations between Two- and Three-Dimensional Local Porosity Distributions for Natural and Artificial Porous Media. *Physica A*, 232, 1–20.
- Wallerstein, N. P., Thorne, C. R. & Doyle, M. W., 1997. Spatial distribution and impact of large woody debris in northern Mississippi. *Management of Landscapes Disturbed by Channel Incision*, Wang S.S.Y., Langendoen E.J., Shields F.D. (eds). University of Mississippi: Mississippi, USA, 145–150.
- Wang, R., Peethambaran, J., Chen, D., 2018. LiDAR Point Clouds to 3-D Urban Models: A Review. *IEEE Journal of Selected Topics in Applied Earth Observations and Remote Sensing* 11, 606–627.
- Warren, D.R., Kraft, C.E., Keeton, W.S., Nunery, J.S., Likens, G.E., 2009. Dynamics of wood recruitment in streams of the northeastern US. *For. Ecol. Manag.* 258, 804–813.
- Webb, A.A., Erskine, W.D., 2003. Distribution, recruitment, and geomorphic significance of large woody debris in an alluvial forest stream: Tonghi Creek, southeastern Australia. *Geomorphology* 51, 109–126.
- Welber, M., Bertoldi, W., Tubino, M., 2013. Wood dispersal in braided streams: results from physical modeling. *Water Resour. Res.* 49, 7388–7400.
- Westoby, M.J., Brasington, J., Glasser, N.F., Hambrey, M.J., Reynolds, J.M., 2012. 'Structure-from-Motion' photogrammetry: a low-cost, effective tool for geoscience applications. *Geomorphology* 179, 300–314.
- Wohl, E., Scott, D.N., 2017. Wood and sediment storage and dynamics in river corridors. *Earth Surf. Process. Landf.* 42, 5–23.
- Wohl, E., Bledsoe, B.P., Fausch, K.D., Kramer, N., Bestgen, K.R., Gooseff, M.N., 2016. Management of large wood in streams: an overview and proposed framework for hazard evaluation. *JAWRA Journal of the American Water Resources Association* 52, 315–335.
- Wolff, K., Kim, C., Zimmer, H., Schroers, C., BOTSCH, M., Sorkine-Hornung, O. & Sorkine-Hornung, A., 2016. Point cloud noise and outlier removal for image-based 3D reconstruction. 118–127.
- Wright, A., Marcus, W.A., Aspinall, R., 2000. Evaluation of multispectral, fine scale digital imagery as a tool for mapping stream morphology. *Geomorphology* 33, 107–120.
- Zhang, W., Thompson, K.E., Reed, A.H., Beenken, L., 2006. Relationship between packing structure and porosity in fixed beds of equilateral cylindrical particles. *Chem. Eng. Sci.* 61, 8060–8074.
- Zou, R.P., Yu, A.B., 1996. Evaluation of the packing characteristics of mono-sized non-spherical particles. *Powder Technol.* 88, 71–79.